Macromolecular Bioscience
www.mbs-journal.de

Flexible and Biocompatible Antifouling Polyurethane Surfaces Incorporating Tethered Antimicrobial Peptides through Click Reactions

*Mattias Berglin, Jorunn Pauline Cavanagh, Josefin Seth Caous, Balmukund Sureshkumar Thakkar, Jeddah Marie Vasquez, Wenche Stensen, Benny Lyvén, John-Sigurd Svendsen, and Johan Svenson**

Efficient, simple antibacterial materials to combat implant-associated infections are much in demand. Herein, the development of polyurethanes, both cross-linked thermoset and flexible and versatile thermoplastic, suitable for "click on demand" attachment of antibacterial compounds enabled via incorporation of an alkyne-containing diol monomer in the polymer backbone, is described. By employing different polyolic polytetrahydrofurans, isocyanates, and chain extenders, a robust and flexible material comparable to commercial thermoplastic polyurethane is prepared. A series of short synthetic antimicrobial peptides are designed, synthesized, and covalently attached in a single coupling step to generate a homogenous coating. The lead material is shown to be biocompatible and does not display any toxicity against either mouse fibroblasts or reconstructed human epidermis according to ISO and OECD guidelines. The repelling performance of the peptide-coated materials is illustrated against colonization and biofilm formation by *Staphylococcus aureus* and *Staphylococcus epidermidis* on coated plastic films and finally, on coated commercial central venous catheters employing LIVE/DEAD staining, confocal laser scanning microscopy, and bacterial counts. This study presents the successful development of a versatile and scalable polyurethane with the potential for use in the medical field to reduce the impact of bacterial biofilms.

1. Introduction

Healthcare costs represent major expenses for any country, and it has been estimated that the US healthcare system accounts for nearly 20% of the nation's economy.[1] Infections caused by multiresistant pathogens represent a significant contribution to the burden of the healthcare system, both from an economic and a human perspective.[2–5] One challenging area where infections lead to extensive patient suffering is those associated with bacterial biofilms, implants, and invasive medical devices.[5–8] Even with the advances made in minimally invasive surgery and aseptic techniques, infections associated with medical device implantation remain a common complication.[6,9,10] Clinically, unsuccessful treatment often leads to costly and painful replacement surgery and extended patient suffering.[9,11] Other common, and potentially fatal conditions such as urinary tract infection[12] (UTI), ventilator-associated pneumonia,[13] and catheter-related bloodstream infection[5,14] are often

M. Berglin, J. S. Caous, J. M. Vasquez, B. Lyvén, J. Svenson[+]
Department of Materials and Production
RISE Research Institutes of Sweden
Gothenburg 413 46, Sweden
E-mail: johan.svenson@cawthron.org.nz

The ORCID identification number(s) for the author(s) of this article can be found under https://doi.org/10.1002/mabi.202300425

[+]Present address: Cawthron Institute, Nelson 7010, New Zealand

DOI: 10.1002/mabi.202300425

M. Berglin
Department of Chemistry and Molecular Biology
Gothenburg University
Gothenburg 413 90, Sweden

J. P. Cavanagh, B. S. Thakkar, J.-S. Svendsen
Amicoat A/S
Oslo Science Park, Oslo 1386, Norway

J. P. Cavanagh
Department of Clinical Medicine
UiT The Arctic University of Norway
Tromsø 9019, Norway

W. Stensen, J.-S. Svendsen
Department of Chemistry
UiT The Arctic University of Norway
Tromsø 9019, Norway

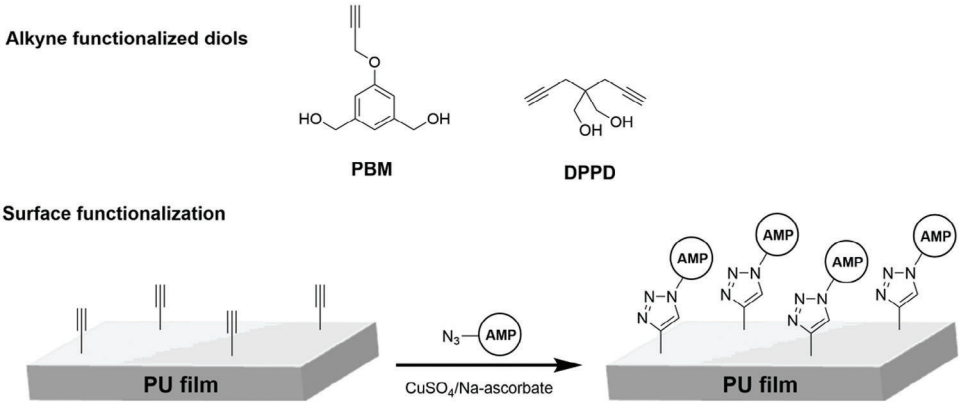

Figure 1. Top: Alkyne functionalized diols developed by Du Prez and co-workers[49] and evaluated in the current project. Bottom image: Schematic representation of click-mediated AMP functionalization of a PU-film incorporating alkyne-containing monomers.

directly linked to the formation of bacterial biofilms on catheter surfaces.[15–17] While critically ill patients are most affected by infections associated with medical devices, ≈75% of nosocomial UTIs are associated with indwelling urinary catheters,[18] which are employed during the treatment of 12–21% of all hospitalized patients.[19]

Apart from limiting the unnecessary use of catheters,[20] other options that have been evaluated to prevent or limit the extent of bacterial colonization include smart functionalized coatings that act either as direct bacterial killers or as settlement repellents.[7,21,22] For example, incorporating a slow-release antibiotic into the implant or coating via hydrolytically degradable multilayers or by bonding to graphene that sequentially delivers the antibiotic has been shown to increase tissue integration and lower infection occurrence.[21,23,24] ZnO nanorods, superhydrophobic surfaces, and noble metal nanoparticles have also all been evaluated for their use in preventing the formation of bacterial biofilm on medical devices and implants.[21,22,25,26]

While many of the methods depend on the release[27,28] of an antibacterial component, an increasing number of studies are also focusing on developing coatings that incorporate elements from the innate immune system,[29,30] as recently reviewed by Negut and co-workers.[31] These strategies rely on surface grafting of antimicrobial peptides (AMPs), whereby the peptide provides either a repelling, bacteriostatic, or bactericidal activity that prevents bacterial colonization.[32–34] Numerous parameters influence the successful tethering of an AMP to a surface while maintaining bioactivity,[35] and recent studies have highlighted their potential.[31,32,36,37]

Synthetically modified AMPs can be designed with increased stability[38] and improved antibacterial effect,[39,40] and anchoring functionalities can be incorporated into them to allow covalent surface attachments.[31,40] Our recent studies on short mimics of lactoferricin-based AMPs[39] have revealed their high and rapid disinfecting potential when employed in both wound dressings[41] and antifungal cream preparations.[42] Short active AMP mimics are readily prepared[40] and can be well tolerated in vivo, with low irritability or toxicity.[43] As such, they have promising attributes, making them suitable for incorporation into functional coatings[31,35] for medical applications. This is also a strategy that circumvents some of the challenges associated with realizing the potential of AMPs in systemic use.[44–46]

Polyurethane (PU) is commonly used in medical devices and the material is often generated via step-growth polymerization, employing diioscyanates, polyols, and diol chain extenders.[47,48] PU is a versatile material, and the ongoing research into developing antibacterial PU coatings was recently extensively reviewed by Wang and co-workers.[26] Functionalization of PU can be achieved via several methodologies,[26,49,50] and incorporation of a range of functional compounds such as poly(ethylene glycol),[51] monoethylene glycol hydroxide,[52] quaternary ammonium compounds,[53] and zwitterions[54] has been used to reduce bacterial adhesion and growth. Successful examples of a PU combined with AMPs, either via release[55] or covalent coating,[36] have also been published.[26]

For commercial production of medical materials, simplicity is key, and incorporation of functionalized monomers into the polymer synthesis has been shown to be a successful approach for PU functionalization.[49] Alkyne-containing diols have been incorporated in PU films and foams by Du Prez and co-workers[49,56] and by Ott et al.[57] by employing either 3,5-*bis*(hydroxymethyl)−1-propargylbenze (PBM) or 2,2-di(prop-2-ynyl)propane-1,3-diol (DPPD) to present alkyne functionalities, allowing for quantitative surface coupling reactions via click chemistry,[49] as schematically shown in **Figure 1**.

In the current study, we report the development of a novel flexible PU coating that can be readily functionalized with AMPs to generate a protective coating. This relies on tailor-made synthetic AMPs directly covalently linked via copper-catalyzed 1,3-dipolar cycloaddition (CuAAC) chemistry that has been successfully used on other materials.[58,59] Direct peptide coupling circumvents many of the challenges associated with anchoring AMPs that severely limit the production and clinical applicability of the materials.[21] This study includes the development of optimized AMPs for surface attachment, as well as the rational design and evaluation of a novel flexible and biocompatible PU material suitable for medical coating applications beyond the limitations of crosslinked PU previously reported. The active AMPs were coupled to the PU, and the final hybrid materials were extensively characterized physically, mechanically, chemically, and

biologically before being evaluated as functional antibacterial coatings in vitro.

2. Experimental Section

2.1. Peptide Synthesis + Antibacterial Evaluation in Solution In Vitro

Peptides were prepared by Amicoat A/S and used as received. Briefly, AMC-109 was prepared according to literature procedures,[38] while AMC-08-89 and AMC-25-01 were synthesized on 2-chlorotrityl resin and Rink Amide AM resin, respectively, using standard Fmoc-protocols.[60] The PEG-linker was attached to the side chain-protected AMC-08-89 peptide in solution, while the whole AMC-25-01 was assembled on the resin. AMC-25-04 was generated by attaching AMC-109 to a PEG-linker.[61] See Supporting Information for additional information regarding synthesis, including NMR characterizations (Figures S1–S3 and Table S1, Supporting Information). The peptides were purified using reversed-phase HPLC on a Supelco Ascentis C18 column (10 µm, 21.2 × 100 mm), with a mixture of water and acetonitrile (both containing 0.1% trifluoroacetic acid (TFA)) as eluent. The purity of the peptides was analyzed by RP-HPLC using a Supelco Ascentis Express C18 column (2.7 µm, 3.0 × 100 mm) and positive ion electrospray mass spectrometry on a Thermo Orbitrap mass spectrometer.

The minimal inhibitory concentration (MIC) of each peptide was determined against *Staphylococcus aureus* (*S. aureus*, ATCC 29213), *Escherichia coli* (*E. coli*, ATCC 25922), and *Staphylococcus epidermidis* (*S. epidermidis*, RP62a), via serial dilution according to Wiegand et al.[62] Briefly, three to five colonies, from freshly prepared blood agar plates, were grown under shaking conditions in 3 mL Mueller-Hinton Broth (MHB) for two to 6 h to prepare 1×10^7 cfu mL^{-1} stock solutions, as determined by measurements of optical density (OD) at 600 nm. The bacterial suspension was further diluted 1:10 in MHB to generate final inoculums (1×10^6 cfu mL^{-1}), as confirmed by viable count. Peptides were dissolved in dimethyl sulfoxide (DMSO) to a concentration of 20 mg mL^{-1}, serially diluted to suitable concentration (128–2 µg mL^{-1}), and added to microtiter plates (10 µL in each well). The bacterial inoculum (90 µL) was added to each well before the plates were incubated at 37 °C for 20 h in humid environment to obtain satisfactory growth. Bacterial growth was analyzed by visual examination and OD measurement at 600 nm. The MIC was defined as the lowest antimicrobial concentration inhibiting the visible growth of the bacterium investigated (a 50% reduction in OD was set as the limit). Each peptide concentration was analyzed in duplicate. Inoculum, including the highest used concentration of DMSO (0.6%) was used as growth/negative control, DMSO in growth medium was employed as sterility control and blank. Gentamicin sulfate (Sigma Aldrich G1914) and AMC-109 were used as positive controls.

2.2. Polyurethane Synthesis

Poly(tetrahydrofuran) (PTHF) (CAS 25190-06-1, M_w = 950–1050 g $mole^{-1}$ and M_w = 2825–2976 g $mole^{-1}$) and diisocyanates (isophorone diisocyanate (IPDI), CAS 4098-71-9, toluene diisocyanate (TDI), CAS 584-84-9, 4,4′-methylene*bis*(phenyl isocyanate) (MPI), CAS 101-68-8, and hexamethylene diisocyanate (HDI), CAS 822-06-0) were obtained from Sigma Aldrich, Sweden. Glycerol ethoxylate-*co*-propoxylate triol (CAS, 51258-15-2), 1,3-propanediol (CAS, 504-63-2), 2-ethylhexyl diphenyl phosphate (CAS, 1241-94-7), and anhydrous (<50 ppm) dimethylformamide (DMF) were also provided by Sigma Aldrich, Sweden. The dimethyltin dineodecanoate catalyst was provided by Avison GmbH, Germany. The poly(tetrahydrofuran) was dried for 16 h at 60 °C under vacuum prior to use, while the glycerol ethoxylate-*co*-propoxylate triol and diisocyanates were used as received. The 3,5-*bis*(hydroxymethyl)−1-propargylbenze (PBM) and 2,2-di(prop-2-ynyl)propane-1,3-diol (DPPD) chain extenders were received from Amicoat A/S and stored under dry conditions in an exicator before used.

2.3. Cross-Linked Polyurethane

Cross-linked PU films were prepared by adding a controlled amount of PBM and 1,3-propanediol to a glass vial (10 mL). To facilitate polymerization and polymer stability, a triol (glycerol ethoxylate-*co*-propoxylate triol) was added (1.5–2.3 mol%) The mixture was heated to 90 °C while being stirred and then purged with N_2 (g). When a homogenous mixture was attained, isocyanate monomers (IPDI and TDI) were added. The molar ratio between total isocyanate and hydroxyl functional groups was shifted toward isocyanate (1.02–1.05). Polymerization was initiated by adding dimethyltin dineodecanoate catalyst dissolved in 2-ethylhexyl diphenylphosphate, reaching a final concentration of 0.4%. After 10–15 s of mixing, polymer films were prepared on polyester (polyethylene terephthalate, PET, Kodak ESTAR, Rochester, USA) substratum using a 500 µm film applicator. After application, the films were cured at 70 °C for 1 h. Films were extracted in EtOH and acetone, dried at 70 °C overnight, and stored under ambient conditions before being analyzed.

2.4. Flexible Segmented Thermoplastic Polyurethane

For synthesis of the prepolymer, dried PTHF (≈0.005 mol) dissolved in DMF (40 mL) was added to a three-necked round-bottom flask (100 mL) fitted with a burette, condenser, and gas-tight mechanical stirrer. The flask was placed in an oil bath at 80 °C, purged with nitrogen, and stirred with a Teflon blade. Diisocyanate (MDI, TDI, or HDI) was then charged to the flask at an NCO:OH ratio of 2:1. Dimethyltin decanoate catalyst (0.4 w/w% based on total monomer mass) dissolved in DMF (10 mL) was added, and the reaction was carried out until the theoretical isocyanate content was reached, as determined by following the disappearance of the isocyanate absorbance at 2270 cm^{-1} using ATR FT-IR. For the final polymer synthesis, 0.005 mol (molar ratio NCO:OH 1:1) of PBM was dissolved in DMF (10 mL) and added to the prepolymer. Polymerization was carried out at 80 °C under nitrogen purge until a stable molecular mass was reached, as determined by size exclusion chromatography (SEC). The reaction mixture was precipitated in ice-cold Milli-q water, then washed three times in water and once in ethanol.

The finished polymer was dried in a vacuum at 70 °C until stable mass was reached (typically 20–24 h). Thin films (≈25 μm) for characterizations and functionalization were prepared on PET substratum (Kodak ESTAR, Rochester, USA). The PU polymer was dissolved in BHT stabilized (0.025%) tetrahydrofuran (THF, VWR chemicals, France) at 1 w/v%, and films were prepared using a 200 μm film applicator followed by solvent evaporation at ambient RT overnight. Thicker films (≈250 μm) were prepared on polytetrafluoroethylene (PTFE) foil (ESSKA, Sweden) using a 10% w/v% PU solution in THF and a 500 μm film applicator. After preparation, solvent was allowed to evaporate for at least 3 days. Before analysis, the PU-film was removed from the PTFE foil and cut into suitable pieces.

2.5. Polymer Characterization

The polymers were evaluated using a suite of spectroscopic and mechanical methods, as described in the supporting material.

2.6. CuAAC Reaction

2.6.1. In Solution

Acetonitrile, TFA, sodium ascorbate salt, and copper sulfate pentahydrate ($CuSO_4 \cdot 5H_2O$) were purchased from Sigma Aldrich, Sweden. PBM and AMC-25-04 were provided by Amicoat AS, Norway. Probing of optimal coupling conditions was performed with ranging concentrations of ascorbic acid and copper sulfate. For a typical solution reaction, 250 μL of aqueous PBM (3.2 mM) was mixed with 250 μL of peptide (3.2 mM), also dissolved in deionized water. Varying amounts of ascorbic acid (0.16–20 mM) and copper sulfate (0.032–3.2 mM) were added as aqueous solutions at 250 μL each to reach a final volume of 1 mL. The reactions were monitored for 40 h at ambient temperatures using a Perkin Elmar Flexar HPLC fitted with a Flexar binary pump. The compounds were separated using gradient elution (from 25% to 40% acetonitrile) over 60 min using mixtures of acetonitrile and deionized water (0.1% TFA in each solvent). Next, 10 μL of the reaction mixture was injected into the column (Quasar C18 column 250 × 4.6 mm inner diameter, 5 μm particle size) and heated at 30 °C in a Flexar Peltier LC Column Oven that housed it. The signal was detected and processed with a Flexar PDA Plus Detector with a 10 mm flow cell. Data were collected at both 254 and 280 nm, with the data processed primarily being from the 254 nm readings. Verification and quantification of the formation of the solution click products were also performed using MS. The samples were separated by LC (Acquity UPLC I Class, Waters) using an Acquity UPLC CSHT C18 1.7 μm column at 70 °C. The gradient employed was from 95:5 of 0.1% formic acid 0.05% TFA in water:0.1% formic acid 0.05% TFA in acetonitrile to 5:95 in 2 min at a flow rate of 0.8 mL min^{-1}. The analytes were detected by ESI in positive ion mode by MS (G2-S QTOF, Waters) and data were evaluated using the MassLynx 2.1 (Waters) software.

2.6.2. On Alkyne Functionalized PU

The conditions for coupling peptide to the PU films with different compositions were investigated to find conditions yielding a reproducible, stable, and flexible PU material. The functionalization was carried out according to the following general protocol. Pieces of PU film were prepared and placed in an Eppendorf tube. The PU films were washed first in EtOH for 5 min, followed by Milli-Q water (3 × 5 min). The Cu (II) solution, the ascorbic acid, and the peptide solution were then added to the tube. The Cu concentration was varied between 2 and 1000 nM, the ascorbate concentration between 4 and 2000 nM, and the peptide concentration between 0.05 and 10 μM. After a controlled time period at ambient room temperature (RT), the reactants were removed and the PU films were washed in Milli-Q water (3 × 5 min). The films were allowed to dry in RT for 1 h before being refrigerated until further tests. For most coating experiments, a molar ratio of peptide:$CuSO_4$:ascorbic acid of 1:2:10 with overnight incubation was employed. The presence of peptide on the prepared surfaces was verified using X-ray photoelectron spectroscopy (XPS), time-of-flight secondary ion mass spectrometry (ToF-SIMS), static contact angle measurements, and quartz crystal microbalance with dissipation monitoring (QCM-D).

2.7. Biocompatibility According to ISO 10993 and ISO/TC 194/WG 8

2.7.1. Fibroblasts

MTT cytotoxicity tests were performed on L929 mouse fibroblasts. Polymer films were extracted, and the cytotoxicity of the leachates was assessed according to ISO 10993-5:2009 Annex C. Polymer pieces 10 × 20 mm (100 μm thick) were employed for the cytotoxicity assay. Briefly, for the cytotoxicity test, two concentrations of the polymer extract (100% and 50%) were used together with positive control (latex rubber) and negative control (Thermanox Plastic Coverslips) extracts. All dilutions were performed with blanks (extraction vehicle not containing the test item but subjected to conditions identical to those to which the test item was subjected during extraction). Each extract solution was added to six replicate wells containing a subconfluent monolayer of L929 cells. Blanks were also placed in six wells on each side of the 96-well plate to confirm that no systematic cell seeding errors occurred, as well as to serve as a 100% measure of cell viability. After the extracts were added, the plate was incubated for 24 h at 37 ± 1 °C in 5 ± 1% CO_2. Following incubation, the extracts were removed, MTT solution was added to each well, and the cells were incubated for 2 h at 37 ± 1 °C in 5 ± 1% CO_2. After incubation, the MTT solution was removed and 2-propanol was added to each well. The plate was then shaken rapidly until the formazan from the cells had been extracted and formed a homogeneous solution on which the absorbance was measured at 570 nm (reference wavelength 650 nm) to quantify cell viability.

2.7.2. Reconstructed Human Epidermis

Human skin models (reconstructed epidermis) were obtained from MatTek In Vitro Life Science Laboratories. The skin models were shipped at 4 °C on transporting agarose and were used within 96 h of arrival according to manufacturer certification and specification. Before use, the tissues were removed from the

agarose and placed individually in each well of a sufficient number of six-well plates pre-filled with EpiDerm assay medium. They were then placed in an incubator for 60 ± 5 min (37 ± 1 °C and 5 ± 1% CO_2). At the end of the 60-min incubation period, the medium in the wells was removed and replaced with fresh medium. The tissues were then incubated (37 ± 1 °C and 5 ± 1% CO_2) overnight to allow the tissues to recover from transportation. Polymer extracts were prepared in amber glass vials. The polymers were extracted in saline and in sesame oil according to ISO 10993:12-2012, employing the specified ratios of surface area to extraction volume. Extraction was performed at 37 ± 1 °C for 72 ± 2 h with continuous agitation. For the skin irritation test, an exposure time of 18 h was used. Each polymer extract and control were added to three individual skin models (tissues). Saline and sesame oil were employed as negative controls, and 1% SDS solution (in saline) was used as a positive irritant control. The models were incubated at 37 ± 1 °C and 5 ± 1% CO_2. Following incubation, the polymer extracts and controls were removed by extensive washing with DPBS. The washed tissues were transferred to 24-well plates containing MTT solution, where they were incubated for 3 h ± 5 min at 37 ± 1 °C in 5 ± 1% CO_2. After incubation, the MTT solution was removed and the skin models were transferred to 24-well plates pre-filled with 2-propanol and the plates were then sealed to inhibit evaporation. The plates were shaken at 120 rpm for 2 h to allow complete extraction of formazan from the cells. Finally, 200 µL of the solution was pipetted in duplicate into a 96-well plate and the absorbance was measured as described for the fibroblast experiment.

2.8. In Vitro Antibacterial Evaluation of Peptide-Coated Materials

2.8.1. Microscopy Images of Peptide-Coated Surfaces

Overnight colonies of *S. epidermidis* (RP62a) and *S. aureus* (ATCC 29213) in tryptic soy broth (TSB, Sigma Aldrich, Missouri, USA) were used to prepare a 0.5 McFarland (1×10^8 cfu mL^{-1}) suspension and further diluted in TSB with 1% glucose to 10^5 cfu mL^{-1}. Next, 50 µL of bacterial solution was applied to the test material, which was placed in an incubation chamber and incubated at 37 °C for 24 h. After incubation, the test material was rinsed once with PBS by agitation in a well plate, for 5 min, on an orbital shaker (100 rpm). The PBS was exchanged, and the plate was further shaken for 5 min. The films (1 × 3 cm) were left in fresh PBS until stained and imaged. Bacterial viability was evaluated by staining with LIVE/DEAD BacLight Bacterial Viability Kit (Thermo Scientific, Massachusetts, USA). Biofilms were observed using a Leica confocal microscope LSM800 (*S. epidermidis*) and a Zeiss LSM700 confocal microscope (*S. aureus*). Two replicates of each treatment were analyzed at two different positions (150 × 150 µm). The full experiment was repeated once, starting with a new bacterial suspension. Data presented are the grand mean from the two experiments (± 95% confidence interval). Significant differences between control and peptide functionalized surface were evaluated by Mann–Whitney non-parametric unpaired U test. Images were evaluated using ImageJ software (ver. 1.52a, NIH, USA) by first splitting the red and green channels, followed by transformation to binary, and a particle analysis setting cut-off of 5 $pixels^2$ and a circularity of 0.02–1.0. The threshold was set so that orange-colored bacteria were found in the viable (green) channel.

2.8.2. Microscopy Images of Peptide-Coated Catheters

Overnight cultures of *S. epidermidis* RP62a were diluted 1:100 in TSB with 1% glucose. Tubes were cut into 1 cm pieces and further horizontally divided, before being submerged in the bacterial suspension. The coated catheters were incubated overnight, rinsed in PBS, and stained with LIVE/DEAD BacLight Bacterial Viability Kit (Thermo Scientific, Massachusetts, USA). Images were acquired using the ZEISS Axio Zoom V16.

3. Results and Discussion

3.1. Peptide Design

The present study was performed using a bifurcated design, where the peptide part was optimized independently from the PU part. The linker was a short PEG-moiety that was mono- or polydisperse, displaying an azide moiety in one end, while the other end was either modified as an amine (for C-terminal connection of the AMP) or as a carboxylic acid (for N-terminal connection to the AMP). The AMPs were based on truncated versions of bovine lactoferricin that can be structurally simplified by rational design to yield active short peptides composed only of cationic and hydrophobic residues.[39,40] Their chemical and biological properties can be further tuned by incorporating unnatural basic and hydrophobic amino acids.[38,40,63,64] Based on these design principles, a series of peptides were designed and prepared to allow freedom for click-based surface attachment to alkyne-functionalized surface points, as presented in **Figure 2**.

The peptides were selected from two classes, both much shorter than other peptides generally employed in coating studies. The first class was designed from marginally active pentapeptides with a $(WR)_2$-sequence incorporating an additional phenylalanine moiety to improve lipophilicity and, hence, antimicrobial efficacy, as described by Strøm et al.[40,65] The second class was our highly developed and modified tripeptide, AMC-109, where the W in the WR-sequence was replaced by a super-bulky tri-*tert*-butyltryptophan residue, ensuring a very high antimicrobial efficacy.[39] The three peptides H-WRWRFG-NH_2, H-FRWRW-NH_2, and AMC-109 were coupled to the corresponding linker molecules, resulting in AMC-08-89 (monodisperse), AMC-25-01 (monodisperse), and AMC-25-04 (mono- and polydisperse), respectively (Figure 2). The antibacterial effect of the parent peptide and the PEG-linker modified peptides was evaluated in vitro and is presented in Table S2, Supporting Information.

While, in theory, all the included peptides fulfill the structural criteria essential for antimicrobial activity,[40] it is clear that incorporation of the anchoring linker reduces their ability to eradicate bacteria in solution. Both WRWRFG-NH_2 and FRWRW-NH_2, incorporating only natural elements, are moderately active, showing good alignment with previous studies, with reported MIC values of 10–100 µg mL^{-1}.[65,66] With the PEG-linker attached, however, both AMC-08-89 and AMC-25-01 can be regarded as inactive in solution. A reduction in antimicrobial activity has previously been observed for pegylated AMPs, and our results emphasize that this effect is more pronounced for these short AMPs.[67]

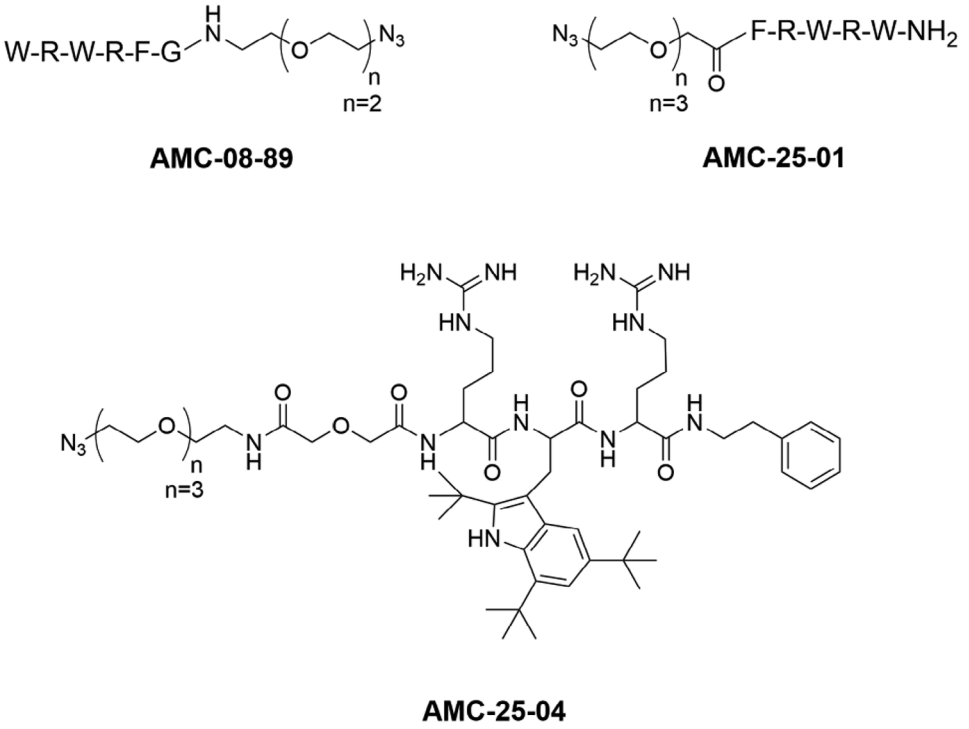

Figure 2. Structure of the different PEG-linked AMPs prepared during the study.

For longer AMPs, increased activity upon PEG-ylation has been observed[68] and it has also been shown that PU modified with pendant PEG groups can display antifouling properties.[69] It is possible that the peptides aggregate in solution due to their PEG-chains and are thus unavailable for interaction with the bacteria in solution.[70] Also, for the highly potent AMC-109, a four-fold reduction in activity upon PEG-ylation was observed (from 4 to 16 μg mL^{-1} against *S. epidermidis*), compared to the "native" peptide.[42] Nevertheless, given the high initial antimicrobial activity of AMC-109, AMC-25-04 remained highly active, with MIC values of 16–64 μg mL^{-1} against the included bacterial strains with either a mono- or a polydisperse PEG-linker. Based on the in vitro solution experiments, it was decided that AMC-25-04 is suited for surface attachment and that the majority of the material studies should be devoted to employing it as a bioactive peptide component. Nevertheless, other selected peptides were also included in specific biological and fundamental material studies in vitro as peptide coupling references and model compounds.

3.2. Click Chemistry in Solution

The ability to couple the azide-functionalized peptides with the alkyne-functionalized PBM monomer was established for peptides AMC-08-89, AMC-25-01, and AMC-25-04 employing the CuAAC reaction.[71,72] The formation of the 1,4-triazole click products was subsequently followed by RP-HPLC and LC-MS (Figures S4 and S5, Supporting Information). The formation of the PBM-peptide conjugate in solution was rapid (<10 min) at optimized reaction conditions, and these were also employed in the 2D polymer format to attach the peptide to the polymerized PBM.[49,56] Verification of covalent peptide attachment to the polymers was established with XPS, Tof-SIMS, static contact angle measurements, and reaction conditions, and quantification was studied with QCM-D, as recently described.[32]

3.3. Polyurethane Design (PU1–PU8), Polymerization, and Characterizations of PU1–PU4

For several medical applications, it is imperative that the PU material is both durable and flexible.[47,48] Initial experiments were thus focused on creating cross-linked materials (**PU1–PU4**) with ranging mechanical and chemical properties incorporating the PBM and DPPD monomers for peptide attachment according to the methodology described by Fournier and Du Prez.[49] A further series of flexible thermoplastic polymers (**PU5–PU8**) were prepared using different isocyanates, hydroxyls, and polyols chain extenders.[73] A range of PU materials of different compositions was generated during the optimization and development (data not shown). Selected key materials that were advanced are presented in **Table 1**. A control material (**PU1**) and three different cross-linked PU polymers (**PU2–PU4**) with variability in the loading of PBM and DPPD were prepared. The incorporation of PBM and DPPD into the polymer was followed by infrared (IR) spectroscopy, with the IR spectrum displaying the expected absorbances.[49,74] The specific alkyne C—H bend absorption found at 847 cm^{-1} in PBM and at 647 cm^{-1} in DPPD could be followed during polymer synthesis. The previously employed PBM alkyne C—H stretch (C≡C—H) at 3290 cm^{-1} could not be employed to follow the reaction events in these systems.[49] The cross-linked PU films demonstrated a linear correlation between

Table 1. Composition of key developed and evaluated PU systems.

	Composition feed [mol%]								
	Chain extender			Isocyanate				PTHF Polyol	
Polymer	PBM or DPPD	Diol[a)]	Triol[b)]	IPDI	TDI	MDI	HDI	1000	2900
PU1	0.0	46.7	2.3	22.0	29.0				
PU2	13.3	37.3	2.1	20.5	26.5				
PU3	32.1	14.5	2.3	22.3	28.5				
PU4	63.4	0.0	1.5	15.2	19.7				
PU5	25.0						50.0	25.0	
PU6	25.0						50.0		25.0
PU7	25.0					50.0			25.0
PU8	25.0				50.0				25.0

[a)] 1,3-propanediol; [b)] Glycerol ethoxylate-*co*-propoxylate triol.

composition of monomer feed and absorption (Figure S6, Supporting Information).

The IR observations indicate that the monomer feed represents the stoichiometric composition of the upper 1–5 µm of the prepared PU films and supports incorporation of PBM and DPPD monomers in the polymer. It was noticed that DPPD-containing polymers displayed a higher mass loss upon wash/extraction in acetone/EtOH (data not shown). Also, the polymer became opaque during functionalization with peptide, indicating higher water uptake. No protocols for optimization in polymerization were pursued, and DPPD-containing polymers were omitted from further characterizations in this study.

The contact angle measurement is more surface sensitive than FT-IR and reflects the topmost surface chemistry, making it possible to assess eventual differences in surface composition as a function of monomer feed. The static contact angle of the films increased from 50.2° ± 0.7 (**PU1**) to 62.6° ± 1.0 (**PU4**) (**Table 2**). This increase is expected with higher PBM in the feed as the aryl group is more hydrophobic than the propyl. This result also supports a relation between monomer feed and surface composition.

The Buchholz hardness of **PU1**–**PU4** increased from 68 ± 1.2 mm^{-1} (**PU2**) to 98 ± 3.9 mm^{-1} (**PU4**), with increased molar fraction of PBM in the monomer feed (Table 2). The **PU4** polymer was hard and glossy, with comparable Buchholz hardness as an epoxy coating, while **PU3** and **PU2** polymers, with a higher content of 1,3-propanediol, were somewhat flexible but still rigid and hard.[75]

Table 2. Static water contact angle, Buchholz hardness, and glass transition temperature T_g of polymers **PU1**–**PU4**.

Polymer	Contact angle [deg][a)]	BR [mm^{-1}][b)]	Glass transition T_g [deg][c)]
PU1	50.2 ± 0.7	68 ± 1.2	n.d.
PU2	56.5 ± 0.8	71 ± 1.7	39.9
PU3	57.0 ± 2.0	82 ± 4.7	50.8
PU4	62.6 ± 1.0	98 ± 3.9	51.2

[a)] All values presented are means of six measurements; [b)] All values presented are means of five measurements; [c)] All values presented are means of two measurements; n.d. = not detected; Error = 95% conf. int.

Glass transition temperatures (T_g) were investigated from 0 to 120 °C, including the important range around 37 °C, at which phase transitions resulting in higher polymer chain flexibility could have a profound effect on biology[76] (Table 2). The T_g increased with increasing content of PBM in the polymer, ranging from 39.9 °C (**PU2**) to 50.8 °C (**PU3**) and up to 51.2 °C (**PU4**). T_g is a bulk property and it is well established that T_g at the surface is reduced.[77] Assuming a decrease in surface T_g of 10 °C would result in T_g of ≈39 °C for the **PU3** polymer and 42 °C for the **PU4** polymer. All polymers should thereby have large chain segmental movements at 37 °C, allowing a higher degree of freedom for peptide alignment and presentation upon interaction with bacterial cell membrane, which could be important for the efficacy of immobilized AMPs. During a 90° bending test, **PU4** polymer showed cracks and delamination from the PET substratum (data not shown). Neither **PU3** nor **PU2** showed this fracture behavior and could thus be more suitable for practical medical applications.

The uniform distribution of alkyne-containing moieties on the µm scale was further assessed on polymers **PU2**–**PU4** using ToF-SIMS. As can be seen in **Figure 3**, no phase separations (within the resolution limit, ≈1 µm2) were found when representative mass fragments originating from different polymer components, that is, PEG fragments from the glycerol ethoxylate-*co*-propoxylate triol cross-linker and aromatic fragments originating from the toluene diisocyanate and PBM monomer, are plotted. No difference in concentration of aromatic fragments between polymers **PU2**–**PU4** could be seen with ToF-SIMS and PBM was shown to be homogenously presented at the interface.

3.4. Coupling of Peptide and Antimicrobial Assessment PU2–PU4

PU3 was selected for antimicrobial coating and efficacy studies, and polymer films were functionalized with peptide AMC-08-89. Upon peptide attachment, the contact angle increased from an initial 57.0° ± 2.0 up to 61.2° ± 1.9. Although statistically verified ($p = 0.01$, *t*-test assuming equal variances), the change does not conclusively verify peptide attachment to the surface. Attempts to characterize the peptide attachment and distribution by Tof-SIMS were unsuccessful as fragments from the peptide and PU

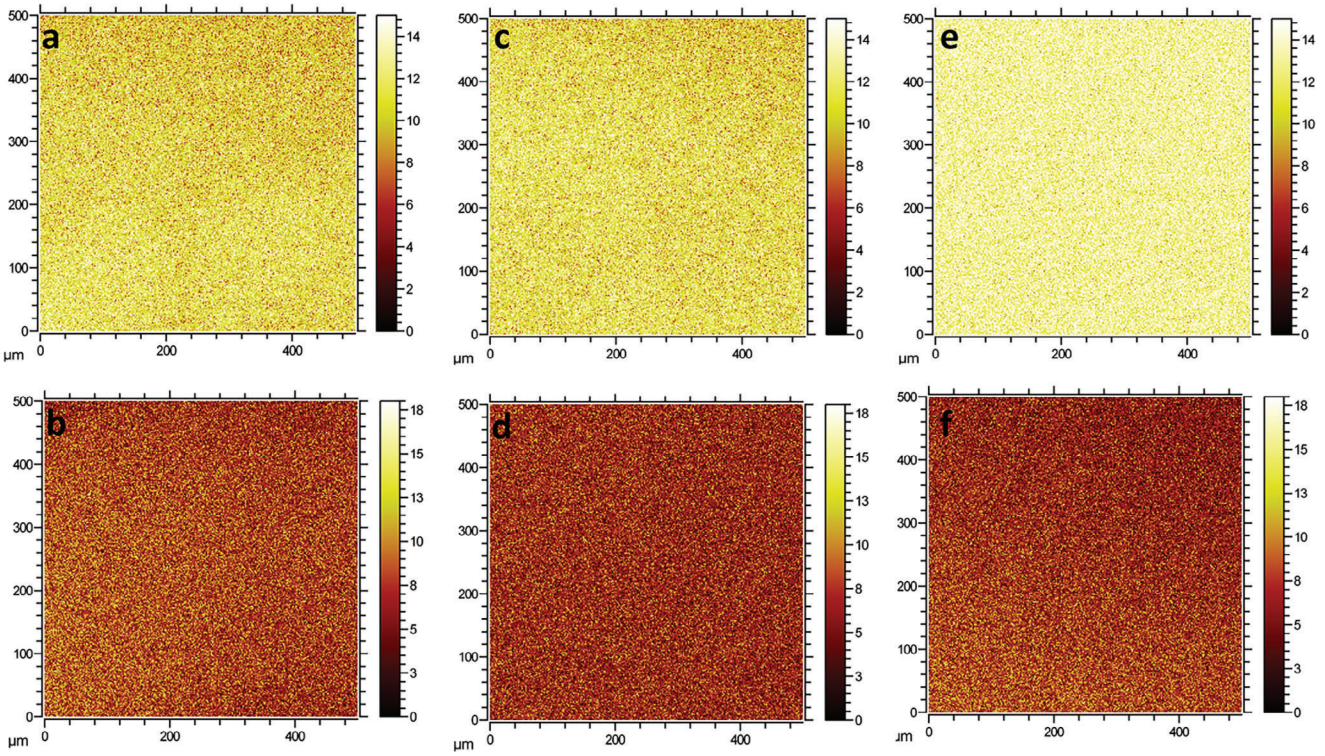

Figure 3. ToF-SIMS mass images of PBM-containing polymers **PU2**–**PU4**. The ion image of mass fragment $C_2H_5O^+$ originating from PEG in polymers **PU2**, **PU3**, and **PU4** is shown in (a), (c), and (e). The ion image of mass fragment $C_6H_5^+$ originating from the PBM and TDI in polymers **PU2**, **PU3**, and **PU4** is shown in (b), (d), and (f), respectively.

were confounded and no specific peptide fragment could be identified (Figures S7 and S8, Supporting Information). However, the rapid and selective coupling between the PBM monomer and peptides, as shown by HPLC and the increased contact angle, potentially induced by the hydrophobic amino acids Trp and Phe in the peptide, support covalent attachment of AMC-08-89 to the PU surface.

The antimicrobial efficacy was assessed by performing a live/dead stain of attached bacteria, visualized by confocal microscopy, images are shown in **Figure 4**a,b. On the **PU3** control surfaces (no peptide), 11–16 bacteria per 100 μm2 were observed, compared with 2–6 bacteria per 100 μm2 on peptide-functionalized surfaces. This represents a significantly lower degree of viable bacteria on the AMC-08-89 functionalized surfaces,

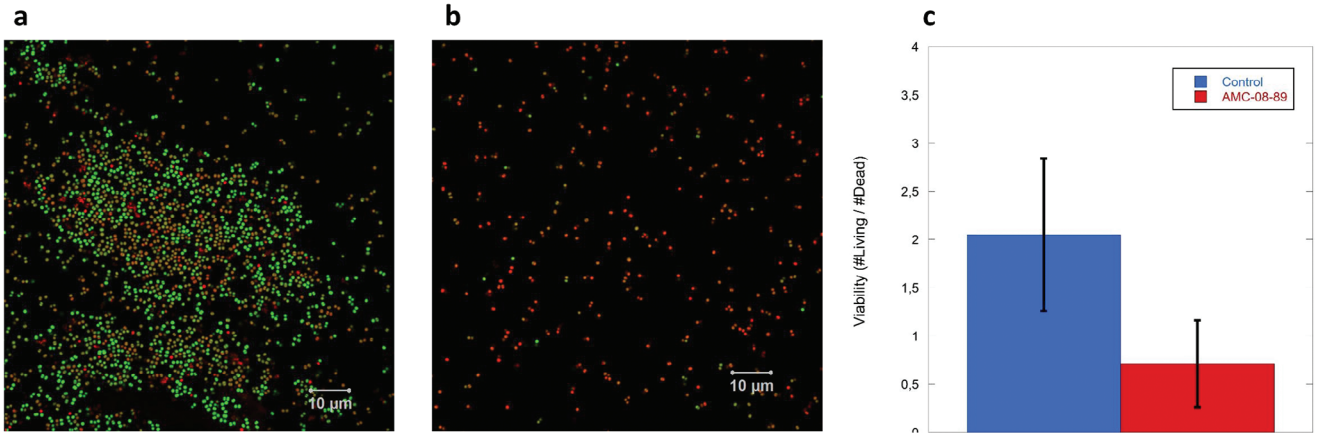

Figure 4. Confocal microscopy images (150 × 150 μm) showing the viability of bacterial cells (*Staphylococcus aureus* ATCC 29213) attached to a) control **PU3** surface and b) AMC-08-89 functionalized **PU3** surface. Data are summarized to show the ratio of viable (green) to non-viable cells (red) on the c) control and the AMC-08-89 functionalized **PU3** polymer.

Table 3. Molecular mass and Buchholz indentation resistance.

Polymer	Contact angle [deg][a)]	Molecular mass[b)] [g mol^{-1}] (M_n/M_w)	BR [mm^{-1}][c)]
PU5	76.2 ± 3.8	25 400/14 300	41.9 ± 2.1
PU6	80.8 ± 4.9	53 600/38 500	35.8 ± 1.9
PU7	64.7 ± 5.0	51 300/36 000	46.7 ± 2.4
PU8	62.8 ± 8.3	50 600/33 600	48.6 ± 2.3

[a)] All values presented are means of four to six measurements; [b)] All values presented are means of two measurements; [c)] All values presented are means of four measurements; Error being 95% conf. int.

as shown in Figure 4c ($p = 0.01$, Mann–Whitney non-parametric unpaired U test).

The observed antibacterial effect was unexpected based on the high solution MIC value this peptide displayed (Table 1). For this class of short peptides, it appears that the PEG-spacer inhibits optimal interaction with the bacterial cell membrane in solution, and that the 2D format may limit the detrimental effect of the PEG-spacer, allowing the peptide to regain activity when immobilized. This PEG-spacer is important for the surface activity, and efficacy studies on the effect of spacer length of different tethered peptides have been reported.[78,79]

3.5. Polymerization and Characterizations PU5–PU8

Despite the observed initial positive biological results, it was decided to continue with more flexible thermoplastic PU materials (**PU5–PU8**, Table 2) due to the limited processability and flexibility at high PBM concentrations of the initially developed **PU2–PU4** thermoset polymers.[74]

The optimization of the polymerization conditions was monitored by IR spectroscopy following the disappearance of the isocyanate group during the synthesis of the prepolymer and final polymer, as well as the characterization of the final PU films (Figure S9, Supporting Information). The polymerization reaction was also studied by SEC, following the increased molecular mass as a function of polymerization time (Figure S9, Supporting Information). The presence of the alkyne functionality at the interface was further verified by confocal Raman spectroscopy (Figures S10–S12, Supporting Information).

The static contact angle of the films ranged from 62.8 ± 8.3 (**PU8**) to 80.8 ± 4.9 (**PU6**) (**Table 3**). Notable is that two groups were formed in which the two highest contact angles were recorded for the polymers containing HDI (**PU5** and **PU6**), while the aromatic containing polymers (**PU7** and **PU8**) displayed lower contact angles. The molecular mass (number average and weight average) of the polymers is presented in Table 3. The molecular mass of the commercial PU material LaripurLPR 7560, which is a TPU with a shore A hardness of 77 and an elongation at break of 690% according to the manufacturer, was included as reference material. The measured mass was nearly 120 000 g mole^{-1}, which is a common molecular weight for elastomers.[80] The molecular masses of polymers **PU5–PU8** were approximately half that of LaripurLPR 7560, but still in the range that has been reported for TPU materials.[81] **PU5** generated much shorter polymer chains as well as higher dispersity (Table 3).

The hardness of the PU films was investigated by performing the Buchholz indentation test to rationally select the most suitable material for further studies,[82] as shown in Table 3. Polymers **PU5–PU8** displayed hardness ranging between 35.8 ± 1.9 mm^{-1} and 48.6 ± 2.3 mm^{-1}. The new linear materials were much softer and flexible compared to the cross-linked **PU1–PU4**, mainly attributed to the incorporation of softer polyols and the removal of cross-linkers. The HDI isocyanate with high molecular mass PTHF polyol (**PU6**) generated the highest molecular mass of the polymers, as well as being the softest, most flexible PU material made, and was selected for further testing. Coatings of **PU6** were rapidly prepared by dissolving the polymer in, for example, THF, followed by an applicator or spray-coating procedure to a substrate surface.

To verify polymer stability upon heat treatment, **PU6** was exposed to thermogravimetric analysis (TGA), which can provide information about the evaporation of substances with low molecular weight, material decomposition, and chemical reactions.[83] The onset of mass loss in N_2, considered to be an indication of the thermal stability of the polymers, is the same for **PU6** and LPR 7560, and both polymers are stable up to 300 °C (Figure S13, Supporting Information). Two steps of thermal decomposition were observed for the materials, which is in agreement with previous TGA studies of PU.[49,83] In O_2, on the other hand, the thermo-oxidative degradation occurs at lower temperatures for **PU6** compared with commercial-grade TPU (Figure S13, Supporting Information). This can be explained by the assumed addition of stabilizers in LPR 7560 compared with **PU6**, which did not have any added stabilizers. The TGA experiments indicate that the prepared **PU6** displays a similar heat loss profile to the commercial TPU reference, and it appears to be equally stable.

A tensile test on **PU6** measured an elongation at break of 582 ± 83%, which can be compared to 690% as stated for the LPR LaripurLPR TPU reference (Figure S14, Supporting Information). The elastic modulus of **PU6** calculated at the initial linear region of the stress–strain curve was 6.4 ± 2.4 MPa. The tensile strength of an elastomer is often related to the molecular weight of the polymer chains, so a somewhat lower tensile strength compared with commercial polyurethanes that have a higher molecular weight is to be expected.[80] The elastic modulus observed was approximately three orders of magnitude lower than, for example, PMMA,[84] and similar to those reported for other TPU materials.[85] The mechanical properties determined during the tensile testing and the sample specifications are summarized in Table S3, Supporting Information, and a representative stress–strain curve of the **PU6** material is displayed in Figure S15, Supporting Information.

3.6. Coupling of AMP-Linker Peptide Constructs to PU6

To accurately quantify both the kinetics of attachment and final peptide surface density, QCM-D was employed. The changes in surface chemistry after covalent coupling were further assessed by static water contact angle and XPS. Chemical surface imaging was performed by Tof-SIMS. QCM-D has previously been demonstrated for azide-alkyne click couplings and for surface-attached microfouling-repelling AMPs.[32,86] In a typical QCM-D

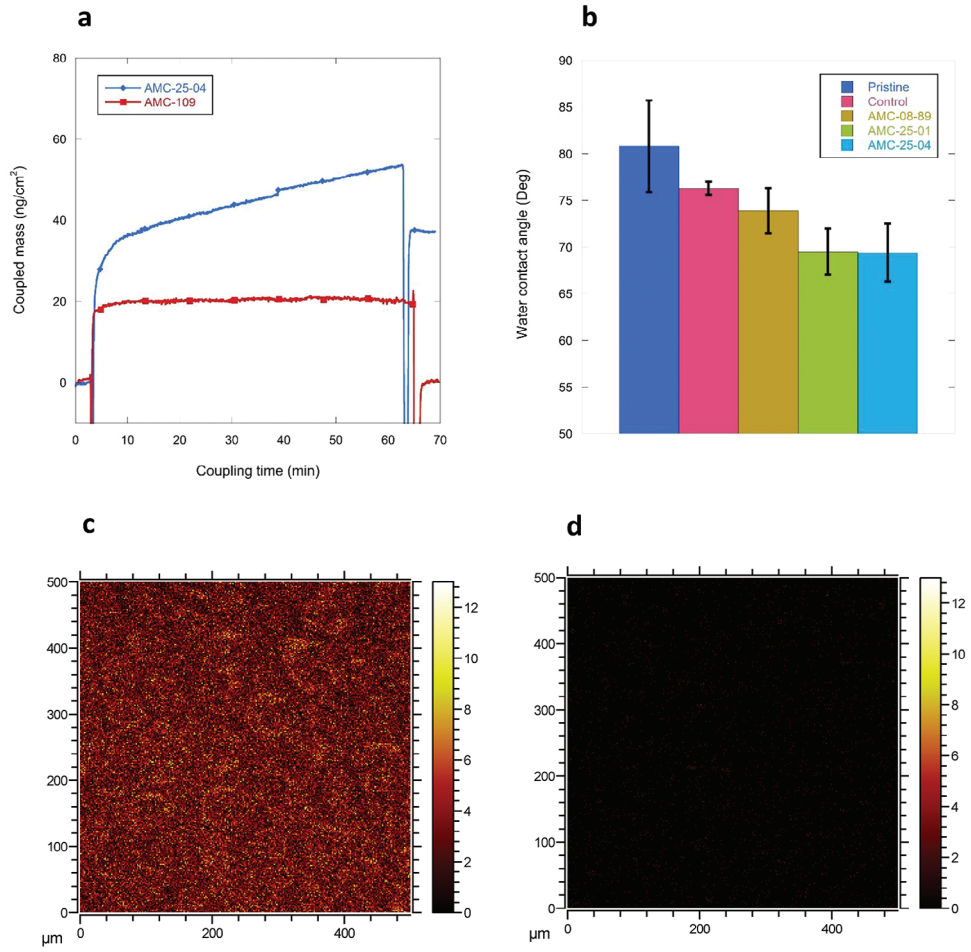

Figure 5. a) Representative QCM-sensorgrams showing the coupling of peptides AMC-25-04 and AMC-109 at 200 μM, 60 min at RT using Cu^{++} 20 μM and ascorbic acid 40 μM. b) Contact angle of **PU6** after coupling using AMC-08-89, AMC-25-01, and AMC-25-04 peptides. Pristine surface is measured on a coating after evaporation of THF solvent (no wash or extraction procedure). Control surface is treated similarly as peptide functionalized surfaces, that is, with ascorbic acid/Cu^{2+}, but peptide was omitted in reactant solution. Contact angle was measured 10 s after drop deposition on surface. Data represent an average of five measurements, with 95% confidence interval. ANOVA was performed to compare the change in contact angle compared with the pristine surface ($p < 0.05$). c) Mass imaging resolving the distribution of peptide peak 298.8 m.u. on **PU6** surface functionalized with AMC-25-04 (500 × 500 μm) d) Mass imaging resolving the distribution of peptide peak 298.8 on control **PU6** surface (500 × 500 μm).

experiment, a rapid increase in associated mass upon injection of a peptide and coupling reagents was observed, as shown in **Figure 5**a. The rapid increase in mass was then followed by a slow, steady increase. The gain in mass could either be physically adsorbed components or covalently bound peptides, or a mixture of both and initial washing (2 mL of buffer) removed about 30% of the non-covalently attached peptide (Figure S16, Supporting Information).

The PU materials currently developed were designed to exert biological effects mediated via a covalently attached peptide[32] and not via peptide release.[55] To verify that the increase in mass upon the CuAAC reaction was not due to non-specific peptide adsorption, further control experiments with AMC-109, lacking the azide functionality needed for click attachment, were performed. As can be seen in Figure 5a, a rapid adsorption of peptide was observed. It is also clear that the peptide was removed in one single washing step, demonstrating the solely non-covalent adsorption to PU. The QCM-D results indicate that AMC-25-04 becomes covalently bonded under click conditions and by varying coupling times and peptide concentrations, surface densities of 3–40 ng cm^{-2} of peptide were measured by QCM-D. These peptide densities are comparable to those reported elsewhere for peptide-coated polymers.[32,37,87]

The contact angle of pristine **PU6** was measured to 89.1° ± 5.6, which is significantly higher than that seen for the previously prepared rigid **PU1–PU4** polymers incorporating PBM at similar molar ratios (Table 2). The higher flexibility of this material allows a higher degree of surface reorganization, exposing more hydrophobic groups toward the interface. Coupling of peptides AMC-08-89, AMC-25-01, and AMC-25-04 to **PU6** (Figure 5b), to the surface lowered the contact angle to around 65–70°. This has previously been seen for immobilized cationic AMPs[88] and indicates that the surfaces become more hydrophilic after peptide attachment. The decrease in contact angle was more pronounced with the peptides AMC-25-01 and AMC-25-04 compared with AMC-08-89 and was significant for all peptides, with *p*-values

ranging from 0.02 (AMC-08-89) down to 0.001 (AMC-25-01 and AMC-25-04). AMC-08-89 (Figure 5b).

The presence of peptide on the surface was further verified by XPS as shown in Figure S17 and Table S4, Supporting Information. After coupling, the atomic composition of the topmost (<10 nm) layer shifted toward higher nitrogen content, reflecting the high nitrogen content of the two guanidine groups present in the peptide. The deconvolution of the C_{1S} carbon peak (Figure S17 and Table S4, Supporting Information) also indicates the presence of the guanidine groups on the surface as both the peak at 286.7 eV (—N—C—N—, C3) and 289.2 eV (CN_3, guanidine, C4) increases after coupling.[89]

Tof-SIMS was employed to verify the homogenous presence of peptide at the polymer–air interface and peptide distribution.[90] ToF-SIMS is an established method for surface characterization and has been used to study and verify surface-coupled peptides in numerous studies.[32,91,92] Reference spectra of AMC-25-04 identified a fragment at 298.8 mu ($C_{21}H_{32}N^+$, Figure S18, Supporting Information). This fragment is believed to originate from the synthetic amino acid tris-*tert*-butyl tryptophan (Tbt) and was selected and used for peptide identification. When the presence of 298.8 mu mass fragment was subsequently analyzed, it could be detected only on polymers where all click reagents had been used, as shown in Figure 5c.

3.7. Evaluation of Biocompatibility

The cytotoxicity of **PU4** and **PU6** (control and peptide functionalized) was evaluated according to ISO standards (ISO 10993–5:2009 Annex C) against L9292 mouse fibroblasts. Peptides AMC-08-89, AMC-25-01, and AMC-25-04 were employed as covalently attached compounds. The flexible **PU6** polymer system was also evaluated as an irritant against human reconstructed epidermis according to OECD TG 439 guidelines, (Table S5, Supporting Information). The L929 cells exposed to the polymer leachates from the two different PU films displayed similar viabilities as those exposed to the negative controls and no cytotoxicity was seen for either the 50% or 100% extracts. A covalent layer of either AMC-08-89, AMC-25-01, or AMC-25-04 did not change the viability of the fibroblasts. **PU6** was also extracted with both saline and sesame oil and evaluated as a potential irritant. The irritation test passed all defined quality controls and according to these test criteria, the **PU6** polymer is neither toxic nor irritant and thus displays a high biocompatibility.

3.8. In Vitro Antibacterial Evaluation

To evaluate the antimicrobial potency of the developed **PU6**, coated and control polymers were inoculated with the biofilm-producing bacterium *S. epidermidis* RP62A. The PU films were prepared on plastic films using an applicator for controlled film thickness, as described in Experimental Section. After incubation, the PU films were rinsed once in PBS and stained with LIVE/DEAD BacLight, and then examined by fluorescence microscopy.[37,41,54] The control surface displayed a well-established live bacterial biofilm after incubation, in contrast to the **PU6** coated with AMC 25-04, which was very sparsely colonized and the bacteria observed were mainly dead (**Figure 6**). The difference in colonization between the materials is substantial and indicates that the optimized AMC-25-04 peptide retains activity when covalently linked and suggests that the anchoring point allows for the peptide to retain a bioactive conformation. Failure to ensure sufficient rotational and structural freedom has been shown to generate surfaces that instead attract bacteria if the immobilized AMPs have not displayed optimal surface conformations.[35,87] Although preliminary, the surface attachment study suggests that the developed polymer is a versatile material for surface attachment of AMPs and that the investigated compound is an interesting lead for coating development. The antibacterial activity of the coated plastic films was not further quantified in this format and additional optimization is expected to yield improved activity, as reported elsewhere for surface-attached Chain201D,[37] Cecropin–Melittin,[93] Mussel-inspired peptides[94] and other efficient, but significantly larger and more complex AMPs.[32,36]

To probe the versatility of this functional antimicrobial layer, a more relevant format was also assessed, employing commercially available lumbar drainage catheters that were coated on the outside and inoculated with bacteria. The catheters were coated with **PU6**-AMC-25-04, and an identical **PU6** film without peptide attached was included as a negative control. Coated catheters were cut into 1 cm pieces cut longitudinally in half and then incubated in *S. epidermidis* overnight cultures that were diluted 1:100 in fresh TSB with glucose. Tubes were incubated for 24 h at 37 °C. After incubation, the tube samples were rinsed with PBS once and stained with LIVE/DEAD BacLight, and then examined by CLSM as shown in Figure 6.

As can be seen in Figure 6, the catheters appear green due to autofluorescence, but the bacterial biofilm is clearly discernible on the control catheter in the top three panels of Figure 6c. As shown in the lower three pictures, no colonization or biofilm formation on the exterior of the peptide-coated catheters was observed. A slight bacterial growth occurs at the inside of the AMC-25-04-coated catheter where there is no peptide coating (in particular, at the ends). The control catheter was heavily colonized with bacteria and a thick biofilm was established. The biofilm was, to a large degree, composed of live (green-colored) bacteria, but dead bacteria were also observed in the images of the control catheters. No accurate quantification could be performed due to the 3D structure of the coated catheter.

4. Conclusions

In the current study, we have developed novel functionalized PU polymers that allow the covalent attachment of short AMPs via click chemistry to combat bacterial colonization and the establishment of bacterial biofilms. Initial experiments using published methodology with cross-linked PU yielded hard and brittle materials at high PBM monomer concentrations with limited processability. This material could find use in thermoset applications, but the mechanical properties may reduce its applicability in the field of medical devices. A change to a novel linear (thermoplastic) polymer allowed the generation of a highly flexible PU material suitable for various coating applications, which opens up a wide range of applications for the polymer. Optimized short and simple azide-functionalized AMPs were successfully tethered to the coatings via a CuAAC reaction in a rapid and

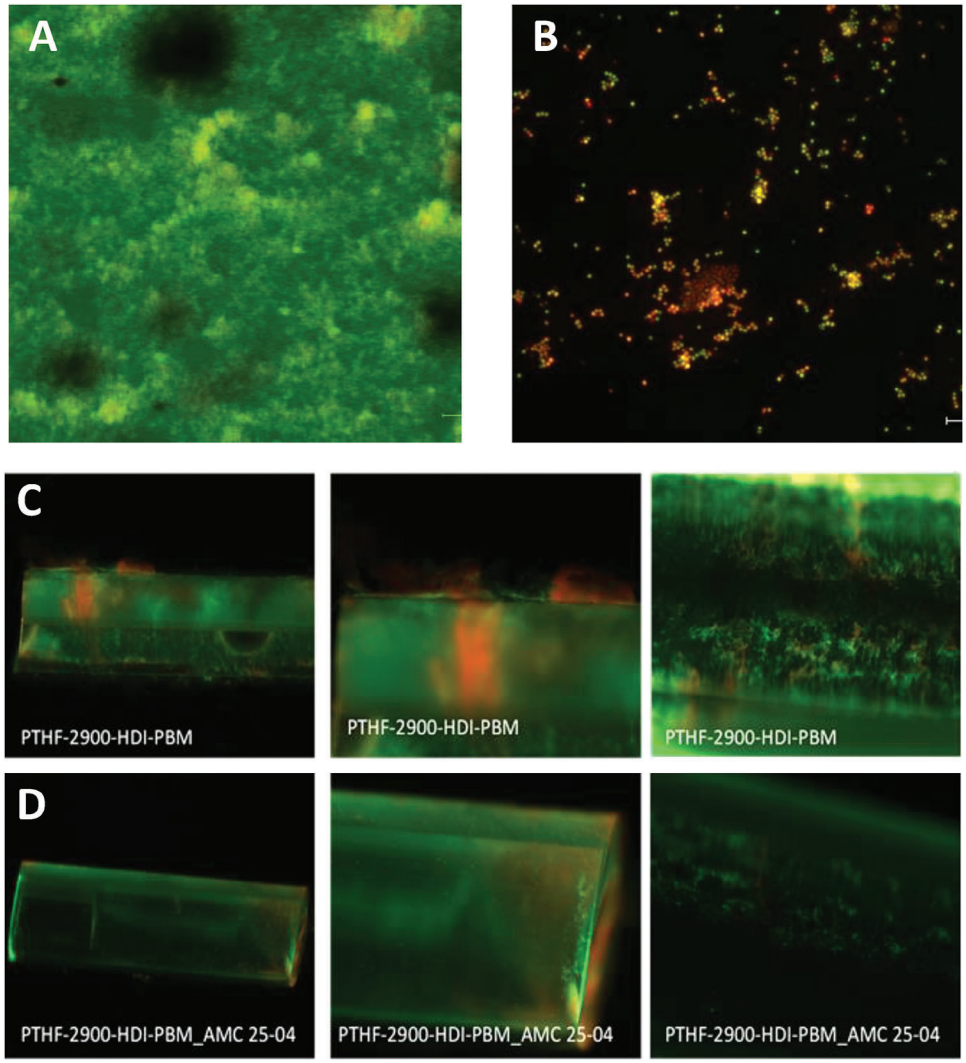

Figure 6. Fluorescence images of coated plastic films after incubation with *S. epidermidis* and fluorescence micrographs of coated PU-catheters. A) Control **PU6** film. B) **PU6** film coated with AMC-25-04 shows a much lower bacterial load. C) Illustration of catheter section coated with **PU6**. D) Catheters coated with **PU6** + AMC-25-04 covalently attached after incubation with *S. epidermidis* and staining.

homogenous fashion to generate uniform peptide surfaces. The prepared AMP-functionalized PU surfaces were shown to be neither toxic nor irritant to mouse fibroblasts or reconstructed human epidermis according to ISO and OECD guidelines. The repelling performance of the peptide-coated materials was illustrated against biofilms of both *S. aureus* and *S. epidermidis* on coated plastic films and was further shown on coated commercial drainage catheters. Overall, the study presents a successful development of a versatile, simple, and biocompatible polymer system with the potential to be used in the medical device field to reduce the impact of bacterial biofilms. Future studies will involve optimization of the antibacterial performance of the coatings and in vivo studies of coated materials.

Supporting Information

Supporting Information is available from the Wiley Online Library or from the author.

Acknowledgements

This study was financed by Amicoat A/S. The authors are grateful for the analytical assistance from RISE scientists L. Brive, P. Borchardt, K. Johansson, and J. Somertune.

Conflict of Interest

J.P.C., W.S., and J.-S.S. are shareholders in Amicoat A/S, which is the company that has financed the study.

Author Contributions

The manuscript was written with contributions from all authors. All authors have given approval to the final version of the manuscript.

Data Availability Statement

The data that support the findings of this study are available in the supporting information of this article.

Keywords

antimicrobial peptide, biocompatible, click chemistry, flexible, polyurethane

Received: September 18, 2023
Revised: October 30, 2023
Published online:

[1] A. M. Sisko, S. P. Keehan, J. A. Poisal, G. A. Cuckler, S. D. Smith, A. J. Madison, K. E. Rennie, J. C. Hardesty, *Health Aff.* **2019**, *38*, 491.
[2] A. Cassini, L. D. Högberg, D. Plachouras, A. Quattrocchi, A. Hoxha, G. S. Simonsen, M. Colomb-Cotinat, M. E. Kretzschmar, B. Devleesschauwer, M. Cecchini, D. A. Ouakrim, T. C. Oliveira, M. J. Struelens, C. Suetens, D. L. Monnet, R. Strauss, K. Mertens, T. Struyf, B. Catry, K. Latour, I. N. Ivanov, E. G. Dobreva, A. Tambic Andrasevic, S. Soprek, A. Budimir, N. Paphitou, H. Zemlicková, S. Schytte Olsen, U. Wolff Sönksen, P. Märtin, et al., *Lancet Infect. Dis.* **2019**, *19*, 56.
[3] R. C. Founou, L. L. Founou, S. Y. Essack, *PLoS One* **2017**, *12*, e0189621.
[4] P. Dadgostar, *Infect. Drug Resist.* **2019**, *12*, 3903.
[5] P. Pronovost, D. Needham, S. Berenholtz, D. Sinopoli, H. Chu, S. Cosgrove, B. Sexton, R. Hyzy, R. Welsh, G. Roth, J. Bander, J. Kepros, C. Goeschel, *N. Engl. J. Med.* **2006**, *355*, 2725.
[6] H. Koo, R. N. Allan, R. P. Howlin, P. Stoodley, L. Hall-Stoodley, *Nat. Rev. Microbiol.* **2017**, *15*, 740.
[7] M. Riool, A. De Breij, J. W. Drijfhout, P. H. Nibbering, S. A. J. Zaat, *Front. Chem.* **2017**, *5*, 63.
[8] Y. Su, J. T. Yrastorza, M. Matis, J. Cusick, S. Zhao, G. Wang, J. Xie, *Adv. Sci.* **2022**, *9*, 2203291.
[9] J. M. Schierholz, J. Beuth, *J. Hosp. Infect.* **2001**, *49*, 87.
[10] W. E. Stamm, *Ann. Intern. Med.* **1978**, *89*, 764.
[11] S. L. Percival, L. Suleman, C. Vuotto, G. Donelli, *J. Med. Microbiol.* **2015**, *64*, 323.
[12] B. Foxman, *Nat. Rev. Urol.* **2010**, *7*, 653.
[13] J. Chastre, J.-Y. Fagon, *Am. J. Respir. Crit. Care Med.* **2002**, *165*, 867.
[14] R. Gahlot, C. Nigam, V. Kumar, G. Yadav, S. Anupurba, R. Gahlot, C. Nigam, V. Kumar, G. Yadav, S. Anupurba, *Int. J. Crit. Illness Inj. Sci* **2014**, *4*, 162.
[15] B. W. Trautner, R. O. Darouiche, *Arch. Intern. Med.* **2004**, *164*, 842.
[16] J. W. Warren, *Int. J. Antimicrob. Agents* **2001**, *17*, 299.
[17] S. S. Magill, J. R. Edwards, W. Bamberg, Z. G. Beldavs, G. Dumyati, M. A. Kainer, R. Lynfield, M. Maloney, L. Mcallister-Hollod, J. Nadle, S. M. Ray, D. L. Thompson, L. E. Wilson, S. K. Fridkin, *N. Engl. J. Med.* **2014**, *370*, 1198.
[18] L. Chuang, P. A. Tambyah, *J. Infect. Chemother.* **2021**, *27*, 1400.
[19] L. Forde, F. Barry, *J. Infect. Prev.* **2018**, *19*, 123.
[20] J. Meddings, M. A. Rogers, S. L. Krein, M. G. Fakih, R. N. Olmsted, S. Saint, *BMJ [Br. Med. J.]* **2014**, *23*, 277.
[21] C. Adlhart, J. Verran, N. F. Azevedo, H. Olmez, M. M. Keinänen-Toivola, I. Gouveia, L. F. Melo, F. Crijns, *J. Hosp. Infect.* **2018**, *99*, 239.
[22] B. Song, E. Zhang, X. Han, H. Zhu, Y. Shi, Z. Cao, *ACS Appl. Mater. Interfaces* **2020**, *12*, 21330.
[23] E. M. Hetrick, M. H. Schoenfisch, *Chem. Soc. Rev.* **2006**, *35*, 780.
[24] X. Zhang, G. Song, H. Qiao, J. Lan, B. Wang, H. Yang, L. Ma, S. Wang, Z. Wang, H. Lin, S. Han, S. Kang, X. Chang, Y. Huang, *Colloids Surf., A* **2020**, *603*, 125223.
[25] S. Rajan, K. Marimuthu, C. Balaji Ayyanar, A. Khan, S. Siengchin, S. Mavinkere Rangappa, *J. Mater. Res. Technol.* **2022**, *18*, 921.
[26] C. Wang, C. Mu, W. Lin, H. Xiao, *Adv. Colloid Interface Sci.* **2020**, *283*, 102235.
[27] N. M. Lai, N. Chaiyakunapruk, N. A. Lai, E. O'Riordan, W. S. C. Pau, S. Saint, *Cochrane Database Syst. Rev.* **2016**, *3*, CD007878.
[28] M. J. Andersen, A. L. Flores-Mireles, *Coatings* **2019**, *10*, 23.
[29] M. Mahlapuu, C. Björn, J. Ekblom, *Crit. Rev. Biotechnol.* **2020**, *40*, 978.
[30] A. Moretta, C. Scieuzo, A. M. Petrone, R. Salvia, M. D. Manniello, A. Franco, D. Lucchetti, A. Vassallo, H. Vogel, A. Sgambato, P. Falabella, *Front. Cell. Infect. Microbiol.* **2021**, *11*, 668632.
[31] I. Negut, B. Bita, A. Groza, *Polymers* **2022**, *14*, 1611.
[32] M. Herzberg, M. Berglin, S. Eliahu, L. Bodin, K. Agrenius, A. Zlotkin, J. Svenson, *ACS Appl. Bio Mater.* **2021**, *4*, 3360.
[33] K. Liu, F. Zhang, Y. Wei, Q. Hu, Q. Luo, C. Chen, J. Wang, L. Yang, R. Luo, Y. Wang, *ACS Appl. Mater. Interfaces* **2021**, *13*, 38947.
[34] Z. Lu, Y. Wu, Z. Cong, Y. Qian, X. Wu, N. Shao, Z. Qiao, H. Zhang, Y. She, K. Chen, H. Xiang, B. Sun, Q. Yu, Y. Yuan, H. Lin, M. Zhu, R. Liu, *Bioact. Mater.* **2021**, *6*, 4531.
[35] A. Andrea, N. Molchanova, H. Jenssen, *Biomolecules* **2018**, *8*, 27.
[36] K. Yu, J. C. Y. Lo, M. Yan, X. Yang, D. E. Brooks, R. E. W. Hancock, D. Lange, J. N. Kizhakkedathu, *Biomaterials* **2017**, *116*, 69.
[37] C. Monteiro, F. Costa, A. M. Pirttilä, M. V. Tejesvi, M. C. L. Martins, *Sci. Rep.* **2019**, *9*, 10753.
[38] J. Svenson, W. Stensen, B.-O. Brandsdal, B. E. Haug, J. Monrad, J. S. Svendsen, *Biochemistry* **2008**, *47*, 3777.
[39] J. S. M. Svendsen, T. M. Grant, D. Rennison, M. A. Brimble, J. Svenson, *Acc. Chem. Res.* **2019**, *52*, 749.
[40] J. Svenson, N. Molchanova, C. I. Schroeder, *Front. Immunol.* **2022**, *13*, 915368.
[41] J. Håkansson, J. P. Cavanagh, W. Stensen, B. Mortensen, J.-S. Svendsen, J. Svenson, *J. Antibiot.* **2021**, *74*, 337.
[42] W. Stensen, R. Turner, M. Brown, N. Kondori, J. S. Svendsen, J. Svenson, *Mol. Pharmaceutics* **2016**, *13*, 3595.
[43] I. Greco, N. Molchanova, E. Holmedal, H. Jenssen, B. D. Hummel, J. L. Watts, J. Håkansson, P. R. Hansen, J. Svenson, *Sci. Rep.* **2020**, *10*, 13206.
[44] H. B. Koo, J. Seo, *Biopolymers* **2019**, *111*, e24122.
[45] G. E. Flaten, G. Kottra, W. Stensen, G. Isaksen, R. Karstad, J. S. Svendsen, H. Daniel, J. Svenson, *J. Med. Chem.* **2011**, *54*, 2422.
[46] J. Svenson, V. Vergote, R. Karstad, C. Burvenich, J. S. Svendsen, B. De Spiegeleer, *J. Pharmacol. Exp. Ther.* **2010**, *332*, 1032.
[47] A. Das, P. Mahanwar, *Adv. Ind. Eng. Polym. Res.* **2020**, *3*, 93.
[48] J. O. Akindoyo, M. D. H. Beg, S. Ghazali, M. R. Islam, N. Jeyaratnam, A. R. Yuvaraj, *RSC Adv.* **2016**, *6*, 114453.
[49] D. Fournier, F. Du Prez, *Macromolecules* **2008**, *41*, 4622.
[50] A. B. Jóźwiak, C. M. Kielty, R. A. Black, *J. Mater. Chem.* **2008**, *18*, 2240.
[51] K. D. Park, Y. S. Kim, D. K. Han, Y. H. Kim, E. H. B. Lee, H. Suh, K. S. Choi, *Biomaterials* **1998**, *19*, 851.
[52] B. De La Franier, D. Asker, D. van denx Berg, B. Hatton, M. Thompson, *Colloids Surf., B* **2021**, *200*, 111579.
[53] Z. K. Zander, P. Chen, Y.-H. Hsu, N. Z. Dreger, L. Savariau, W. C. Mcroy, A. E. Cerchiari, S. D. Chambers, H. A. Barton, M. L. Becker, *Biomaterials* **2018**, *178*, 339.
[54] S. P. Nikam, P. Chen, K. Nettleton, Y.-H. Hsu, M. L. Becker, *Biomacromolecules* **2020**, *21*, 2714.
[55] A.-C. Strömdahl, L. Ignatowicz, G. Petruk, M. Butrym, S. Wasserstrom, A. Schmidtchen, M. Puthia, *Acta Biomater.* **2021**, *128*, 314.
[56] D. Fournier, B. G. De Geest, F. E. Du Prez, *Kobunja Kwahak Kwa Kisul* **2009**, *50*, 5362.
[57] C. Ott, C. D. Easton, T. R. Gengenbach, S. L. Mcarthur, P. A. Gunatillake, *Polym. Chem.* **2011**, *2*, 2782.
[58] J. He, J. Chen, G. Hu, L. Wang, J. Zheng, J. Zhan, Y. Zhu, C. Zhong, X. Shi, S. Liu, Y. Wang, L. Ren, *J. Mater. Chem. B* **2018**, *6*, 68.
[59] J. Chen, Y. Zhu, M. Xiong, G. Hu, J. Zhan, T. Li, L. Wang, Y. Wang, *ACS Biomater. Sci. Eng.* **2018**, *5*, 1034.
[60] I. Coin, M. Beyermann, M. Bienert, *Nat. Protoc.* **2007**, *2*, 3247.

[61] Y. L. Jiang, Y. Zhu, A. B. Moore, K. Miller, A.-M. Broome, *ACS Chem. Neurosci.* **2018**, *9*, 100.
[62] I. Wiegand, K. Hilpert, R. E. W. Hancock, *Nat. Protoc.* **2008**, *3*, 163.
[63] J. Svenson, R. Karstad, G. E. Flaten, B.-O. Brandsdal, M. Brandl, J. S. Svendsen, *Mol. Pharmaceutics* **2009**, *6*, 996.
[64] R. Karstad, G. Isaksen, E. Wynendaele, Y. Guttormsen, B. De Spiegeleer, B.-O. Brandsdal, J. S. Svendsen, J. Svenson, *J. Med. Chem.* **2012**, *55*, 6294.
[65] M. B. Strøm, B. E. Haug, M. L. Skar, W. Stensen, T. Stiberg, J. S. Svendsen, *J. Med. Chem.* **2003**, *46*, 1567.
[66] S. Clark, T. A. Jowitt, L. K. Harris, C. G. Knight, C. B. Dobson, *Nat. Commun.* **2021**, *4*, 605.
[67] M. Bagheri, M. Beyermann, M. Dathe, *Antimicrob. Agents Chemother.* **2009**, *53*, 1132.
[68] S. R. Dennison, S. M. Reddy, L. H. G. Morton, F. Harris, K. Badiani, D. A. Phoenix, *Biochim. Biophys. Acta, Biomembr.* **2022**, *1864*, 183806.
[69] F. Meng, Z. Qiao, Y. Yao, J. Luo, *RSC Adv.* **2018**, *8*, 19642.
[70] C. Chen, F. Pan, S. Zhang, J. Hu, M. Cao, J. Wang, H. Xu, X. Zhao, J. R. Lu, *Biomacromolecules* **2010**, *11*, 402.
[71] H. Nandivada, X. Jiang, J. Lahann, *Adv. Mater.* **2007**, *19*, 2197.
[72] J. E. Moses, A. D. Moorhouse, *Chem. Soc. Rev.* **2007**, *36*, 1249.
[73] K. Kojio, S. Nozaki, A. Takahara, S. Yamasaki, *J. Polym. Res.* **2020**, *27*, 140.
[74] G. Lu, D. M. Kalyon, I. Yilgör, E. Yilgör, *Polym. Eng. Sci.* **2003**, *43*, 1863.
[75] K. Kowalczyk, T. Spychaj, *Prog. Org. Coat.* **2008**, *62*, 425.
[76] M. Berglin, E. Pinori, A. Sellborn, M. Andersson, M. Hulander, H. Elwing, *Langmuir* **2009**, *25*, 5602.
[77] J. D. Andrade, *Surface and Interfacial Aspects of Biomedical Polymers: Volume 1 Surface Chemistry and Physics*, Springer Science & Business Media, Berlin **2012**.
[78] L. C. Shriver-Lake, G. P. Anderson, C. R. Taitt, *Langmuir* **2017**, *33*, 2878.
[79] M. Bagheri, M. Beyermann, M. Dathe, *Bioconjugate Chem.* **2012**, *23*, 66.
[80] S. Xiao, H.-J. Sue, *Polymer* **2019**, *169*, 124.
[81] C. S. Schollenberger, K. Dinbergs, *J. Elastomers Plast.* **1979**, *11*, 58.
[82] E. Broitman, *Tribol Lett* **2017**, *65*, 23.
[83] G. Trovati, E. A. Sanches, S. C. Neto, Y. P. Mascarenhas, G. O. Chierice, *J. Appl. Polym. Sci.* **2010**, *115*, 263.
[84] C. Y. Zhi, Y. Bando, W. L. Wang, C. C. Tang, H. Kuwahara, D. Golberg, *J. Nanomater.* **2008**, *2008*, 642036.
[85] H. J. Qi, M. C. Boyce, *Mech. Mater.* **2005**, *37*, 817.
[86] F. Lin, J. Zheng, J. Yu, J. Zhou, M. L. Becker, *Biomacromolecules* **2013**, *14*, 2857.
[87] F. M. T. A. Costa, S. R. Maia, P. A. C. Gomes, M. C. L. Martins, *Biomaterials* **2015**, *52*, 531.
[88] P. Cao, C. Yuan, J. Xiao, X. He, X. Bai, *Surf. Interface Anal.* **2018**, *50*, 516.
[89] J. S. Stevens, A. C. De Luca, M. Pelendritis, G. Terenghi, S. Downes, S. L. M. Schroeder, *Surf. Interface Anal.* **2013**, *45*, 1238.
[90] A. M. Belu, D. J. Graham, D. G. Castner, *Biomaterials* **2003**, *24*, 3635.
[91] R. Chen, M. D. P. Willcox, N. Cole, K. K. K. Ho, R. Rasul, J. A. Denman, N. Kumar, *Acta Biomater.* **2012**, *8*, 4371.
[92] T. Pauloehrl, A. Welle, M. Bruns, K. Linkert, H. G. Börner, M. Bastmeyer, G. Delaittre, C. Barner-Kowollik, *Angew. Chem.* **2013**, *125*, 9896.
[93] M. M. Querido, H. P. Felgueiras, A. Rai, F. Costa, C. Monteiro, I. Borges, D. Oliveira, L. Ferreira, M. C. L. Martins, *Adv. Mater. Interfaces* **2018**, *5*, 1801390.
[94] Q. Yao, J. Zhang, G. Pan, B. Chen, *ACS Appl. Mater. Interfaces* **2022**, *14*, 36473.